Title

Qualitative and quantitative analysis of the COVID-19 pandemic by a two-side fractional-order compartmental model

Authors

Ma, Weiyuan
Zhao, Yanting
Guo, Lihong
et al.

Publication Date

2022-05-01

DOI

10.1016/j.isatra.2022.01.008

Peer reviewed

Since January 2020 Elsevier has created a COVID-19 resource centre with free information in English and Mandarin on the novel coronavirus COVID-19. The COVID-19 resource centre is hosted on Elsevier Connect, the company's public news and information website.

ISA Transactions 124 (2022) 144–156

Contents lists available at ScienceDirect

ISA Transactions

journal homepage: www.elsevier.com/locate/isatrans

Qualitative and quantitative analysis of the COVID-19 pandemic by a two-side fractional-order compartmental model ☆

Weiyuan Ma [a,*], Yanting Zhao [b], Lihong Guo [c], YangQuan Chen [d]

[a] School of Mathematics and Computer Science, Northwest Minzu University, Lanzhou 730030, China
[b] Department of Automation, University of Science and Technology of China, Hefei 230026, China
[c] Institute of Mathematics, Jilin University, Changchun 130015, China
[d] Mechatronics, Embedded Systems and Automation Lab, University of California, Merced, CA 95343, USA

ARTICLE INFO

Article history:
Received 5 August 2020
Received in revised form 30 August 2021
Accepted 4 January 2022
Available online 12 January 2022

Keywords:
COVID-19
Fractional order
Two-side
Generalized SEIR model
Analysis

ABSTRACT

Global efforts are focused on discussing effective measures for minimizing the impact of COVID-19 on global community. It is clear that the ongoing pandemic of this virus caused an immense threat to public health and economic development. Mathematical models with real data simulations are powerful tools that can identify key factors of pandemic and improve control or mitigation strategies. Compared with integer-order and left-hand side fractional models, two-side fractional models can better capture the state of pandemic spreading. In this paper, two-side fractional models are first proposed to qualitative and quantitative analysis of the COVID-19 pandemic. A basic framework are given for the prediction and analysis of infectious diseases by these types of models. By means of asymptotic stability analysis of disease-free and endemic equilibrium points, basic reproduction number R_0 can be obtained, which is helpful for estimating the severity of an outbreak qualitatively. Sensitivity analysis of R_0 is performed to identify and rank key epidemiological parameters. Based on the real data of the United States, numerical tests reveal that the model with both left-hand side fractional derivative and right-hand side fractional integral terms has a better forecast ability for the epidemic trend in the next ten days. Our extensive computational results also quantitatively reveal that non-pharmaceutical interventions, such as isolation, stay at home, strict control of social distancing, and rapid testing can play an important role in preventing the pandemic of the disease. Thus, the two-side fractional models are proposed in this paper can successfully capture the change rule of COVID-19, which provide a strong tool for understanding and analyzing the trend of the outbreak.

1. Introduction

On December 8, 2019, the first case of COVID-19, which was caused by a new kind of cluster acute respiratory illness, was confirmed in Wuhan, China. The disease spread quickly in China. In February 2020, the epidemic in China passed its peak and was gradually under control. However, new cases began to appear throughout the world. Then the number of the disease has skyrocketed, and the World Heath Organization (WHO) declared COVID-19 as a global pandemic. As of June 21, 2020, more than 8 million confirmed cases of COVID-19, including about 461,000 deaths, were reported to the WHO [1]. Among them, more than 2 million cases were confirmed in the United States, more than 1 million cases were confirmed in Brazil, 584,680 cases were confirmed in the Russian Federation, and 410,461 cases were confirmed in India. The COVID-19 poses a great threat to health and safety of people throughout the world.

With the number of confirmed and deaths cases soared, countries or regions took many different measures to combat COVID-19. But the disease still has a serious impact on global economies and trade. Governments face the urgent challenge of determining an appropriate response. When will the spread of disease peak or stabilize? Which measures can effectively prevent the spread of the disease? When is the right time to adjust the current policy? Qualitative and quantitative analysis of the spread trends and possible measures are extremely important for prevention and control of COVID-19.

A reliable epidemiological model, which consists of a set of coupled differential equations, is a strong tool for simulating mechanism of the spreading trend and how to control the spread of the disease. Many scholars investigated COVID-19 from

☆ This work was supported by the Alianza UCMX Special Funding for Binational Collaboration Addressing COVID-19, the Fundamental Research Funds for the Central Universities (No. 31920210018), and the Innovation Team of Intelligent Computing and Dynamical System Analysis and Application of Northwest Minzu University.
* Corresponding author.
E-mail address: jsmwy@xbmu.edu.cn (W. Ma).

https://doi.org/10.1016/j.isatra.2022.01.008
0019-0578/

different perspectives by classical integer order models [2,3]. Peng et al. [4] developed a generalized Susceptible–Exposed–Infectious–Recovered (SEIR) model to make prediction about the inflection point in China. Yang et al. [5] explored the epidemics trend of COVID-19 in China by modified SEIR model and artificial intelligence. Li et al. [6] estimated the effect of control measures and city lockdowns by conceptual models. Many other models were proposed for COVID-19, such as metapopulation disease transmission model [7] and transmission model [8].

In the above epidemic models, they are assumed that contact rates, transmission and recovery coefficients are constants. Hence the current states do not depend on past historical states at each time, that is, they are memoryless and are called as Markovian processes. However, it was found that the spread and control of infectious diseases cannot be considered as Markovian processes [9,10]. When a disease spreads in population, individual's experience and knowledge of the disease can affect their response. Furthermore, the experience and knowledge do not have the same effect on all stages of the disease transmission. In other words, the earlier memory has less impact on the present situation, while the recent memory has more impact on the present situation. It can be expected that the long memory effect declines more slowly than an exponential decay, more like a power-law decay. Fractional calculus is a powerful tool to observe the effects of long memory effects [11,12]. Fractional calculus has been applied to capture the characteristics of many diseases, such as chronic wasting disease [13] and human respiratory syncytial virus disease [14]. Most recently, fractional calculus has also been used for modeling COVID-19. Xu et al. [15] used a generalized fractional SEIR model to predict the spread trend of COVID-19 in the United States. Lu et al. [16] investigated the dynamic behavior of COVID-19 with the help of a fractional model with inter-city networked coupling effects.

In general, an epidemiological model is described by integer-order differential equations. By transforming the differential equations into Volterra-integral equations, and then adding power law function $\kappa(t-\tau)=\frac{1}{\Gamma(\alpha)}(t-\tau)^{\alpha-1}, \alpha>0$ into integral terms, the current states of the system depend on all past states and exactly how much depend on the size of α. More realistically, different state variables have different power law decay rates α which will lead to two-side fractional models. Therefore, the two-side fractional model can more accurately describe long memory on the macroscopic behavior of epidemic outbreaks. The purpose of this paper is to first propose and study a model with two-side fractional calculus for qualitative and quantitative analysis of the COVID-19. We give a basic framework to design and analyze two-side fractional models. By transforming the integer-order generalized SEIR model into the Volterra-integral equations, and multiplying integrand by power law function, a two-side fractional generalized SEIR model is established. Transformations are designed to convert the two-side fractional system into left-hand side incommensurate fractional systems. The disease free and endemic equilibrium points are computed. Afterwards, the basic reproduction number R_0 is obtained by a locally asymptotically stable analysis and a threshold that determines whether the equilibrium point is stable or not. The Partial Rank Correlation Coefficient (PRCC) values for R_0 show that increasing protection rate is the most effective way to combat COVID-19. By the real data of the United States, the model with both left-hand side fractional derivative and right-hand side fractional integral terms is validated to have a better prediction performance compared with integer order and left-hand side fractional models. Furthermore, we discuss and estimate reasonableness of measures which are taken by governments to control the spreading of the disease.

This paper is arranged as follows. In Section 2, some basic definitions of fractional operators and mathematical properties are given. In Section 3, an augmented SEIR model is briefly introduced, and a two-side fractional model is established. In Section 4, the dynamical analysis and R_0 are discussed. In Section 5, the prediction performance of the model is tested, and measures are analyzed by real data. Conclusions are given in Section 6 .

2. Preliminary definitions and lemmas

Definition 1 (*[11]*)**.** The fractional integral of order $\alpha>0$ for a function $f(t)$ is defined as

$$\mathcal{I}^{\alpha}_{t_0,t}f(t)=\frac{1}{\Gamma(\alpha)}\int_{t_0}^{t}(t-\tau)^{\alpha-1}f(\tau)\mathrm{d}\tau,$$

where $t>t_0$ and $\Gamma(\cdot)$ is the Gamma function.

Definition 2 (*[11]*)**.** For a given function $f(t), t>t_0$, the αth-order Caputo fractional derivative is defined by

$${}_C\mathcal{D}^{\alpha}_{t_0,t}f(t)=\begin{cases}\frac{1}{\Gamma(m-\alpha)}\int_{t_0}^{t}(t-\tau)^{m-\alpha-1}f^{(m)}(\tau)\mathrm{d}\tau,\\ \quad \text{for} \quad m-1<\alpha<m\in\mathbb{Z}^{+},\\ \frac{d^m f(t)}{dt^m},\\ \quad \text{for} \quad \alpha=m.\end{cases}$$

Let $x(t)\in\mathbb{R}^n$ be the solution of the following fractional system:

$${}_C\mathcal{D}^{\alpha}_{t_0,t}x(t)=f(t,x(t)),\quad x(t_0)=x_0, \tag{1}$$

where $t\in[t_0,T](T\leq+\infty), x(t)\in\Omega\subseteq\mathbb{R}^n$, ${}_C\mathcal{D}^{\alpha}_{t_0,t}x(t)=\left({}_C\mathcal{D}^{\alpha_1}_{t_0,t}x_1(t),\ {}_C\mathcal{D}^{\alpha_2}_{t_0,t}x_2(t),\ldots,\ {}_C\mathcal{D}^{\alpha_n}_{t_0,t}x_n(t)\right)^{\top}, 0<\alpha_i<1$ and $f:[t_0,T]\times\Omega\to\mathbb{R}^n$.

Definition 3 (*[17]*)**.** If $\alpha_1=\alpha_2=\cdots=\alpha_n=\alpha$, then we refer to (1) as a commensurate fractional system; otherwise, we refer to (1) as an incommensurate fractional system.

Definition 4 (*[18]*)**.** If the vector $x^*\in\mathbb{R}^n$ satisfies $f(t,x^*)=0$, then x^* is said to an equilibrium point of system (1).

Lemma 1 (*[19]*)**.** *Consider a linear incommensurate fractional system:*

$${}_C\mathcal{D}^{\alpha}_{0,t}x(t)=Ax(t),\quad x(0)=x_0, \tag{2}$$

where $x\in\mathbb{R}^n$, $A\in\mathbb{R}^{n\times n}$ and $\alpha=(\alpha_1,\alpha_2,\ldots,\alpha_n)^{\top}, 0<\alpha_i\leq1$ with $\alpha_i=\frac{n_i}{d_i}$, $\gcd(n_i,d_i)=1$. Let M be the lowest common multiple of the denominators d_i. If all roots λ of the equation $\Delta(\lambda)=\det\left(\mathrm{diag}\left(\lambda^{M\alpha_i}\right)-A\right)=0$ satisfy $|\arg(\lambda)|>\frac{\pi}{2M}$, then the zero solution of system (2) is globally asymptotically stable.

Lemma 2 (*[20]*)**.** *Let $\alpha_1=\alpha_2=\cdots=\alpha_n=\alpha\leq1$ in system (2). If all eigenvalues $\lambda_i, i=1,2,\ldots,n$ of equation $\Delta(\lambda)=\det(\mathrm{diag}(\lambda)-A)=0$ satisfy either the Routh–Hurwitz stability conditions or the conditions $|\arg(\lambda_i)|>\frac{\alpha\pi}{2}, i=1,2,\ldots,n$, then the zero solution of system (2) is asymptotically stable.*

Remark 1. Stability region of equilibrium point of fractional system (2) is larger than the corresponding integer-order system. For example,

$$\begin{cases}{}_C\mathcal{D}^{\alpha}_{0,t}x_1(t)=0.1x_1(t)-x_2(t),\\ {}_C\mathcal{D}^{\alpha}_{0,t}x_2(t)=x_1(t)+0.1x_2(t),\end{cases} \tag{3}$$

where $\alpha\in\mathbb{R}$, $x_1(0)=1$, and $x_2(0)=-1$. Eigenvalues of the characteristic matrix is $\lambda_{1,2}=0.1\pm\mathrm{i}$. When $\alpha=1$, system (3) is an integer-order system and does not satisfy the stability condition in Lemma 2, so it is not asymptotically stable, as shown

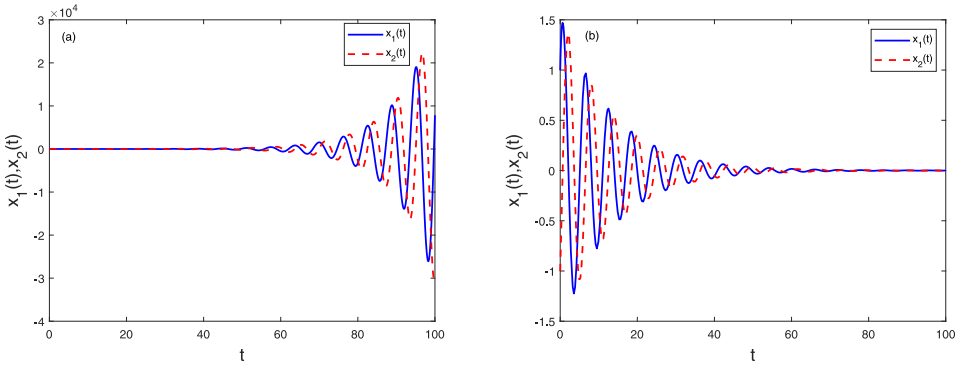

(a) Integer-order system. (b) Fractional system.

Fig. 1. Comparison with asymptotically stable of the integer-order system and the fractional system.

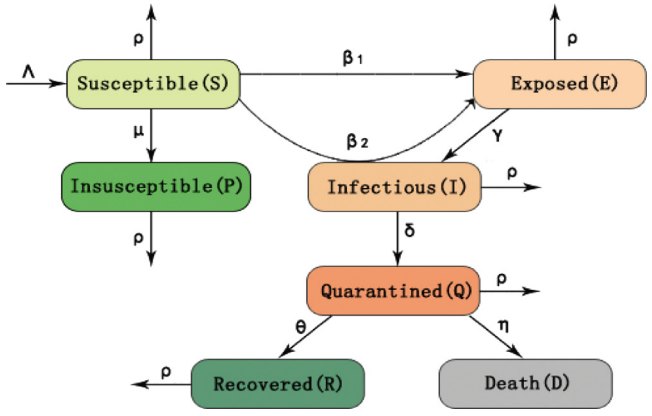

Fig. 2. Flow chart of the model involving seven population classes.

in Fig. 1(a). However, when $\alpha = 0.8$, by Lemma 2, fractional system (3) is asymptotically stable, as shown in Fig. 1(b). Thus, fractional systems are more flexible and consistent with actual situations.

Lemma 3 ([18]). *For any $x_0 = \left(x_1^0, \ldots, x_n^0\right)^\top \in \mathbb{R}^n$, if the function $f(t, x)$ is continuous and satisfies Lipschitz condition with respect to x. Then fractional system (1) has a unique solution.*

3. Model formulation

The pandemic of COVID-19 has had a substantial impact on many aspects of all countries. To control and prevent ongoing outbreak of the diseases, establishing an appropriate model is very important. The total population N is divided into seven classes, i.e., $S(t)$, $E(t)$, $I(t)$, $Q(t)$, $R(t)$ and $P(t)$. Here, $S(t)$ is proportion of the populace that is able to contact the disease, $E(t)$ is proportion of the populace that has been infected but is in a latent period, $I(t)$ is proportion of the populace that has an infectious capacity and has not quarantined, $Q(t)$ is proportion of the populace that is confirmed and infected, $R(t)$ is proportion of the populace that has recovered and become immune, and $P(t)$ is proportion of the populace that is protected from infection. In addition, $D(t)$ is proportion of the populace that has died from the disease.

The flow chart of the generalized SEIR model for COVID-19 and other epidemic diseases is shown in Fig. 2. They represent the interaction rate constants of the different compartments. The

Table 1
Description parameters of the generalized SEIR model (4).

Parameter	Biological meaning
Λ	Inflow rate of susceptible individuals
β_1	Infection rate of the exposed individuals
β_2	Infection rate of the infected individuals
μ	Protection rate
ρ	Natural mortality rate
γ^{-1}	Average latent time
δ^{-1}	Average quarantine time
η	Death rate caused by the disease
θ	Average cure rate

model has nine parameters that can be estimated in numerical simulations and extends the previous model [4,15]. A proportion, μ, of susceptible people are protected from the virus. And the susceptible people (S) move into the exposed people (E) when they are infected by exposed people at the transition rate β_1 or infected people at the transition rate β_2. After that, the exposed individuals (E) move into the infectious people (I) with the transition rate γ. Then, the group I moves into the quarantined individuals (Q) with the transition rate δ. Finally, quarantined people can move into the compartment R at the rate θ due to recovery and may die with the transition rates η. The dynamic behavior of disease can be characterized by the following nonlinear system:

$$\begin{cases} \dfrac{dS(t)}{dt} = \Lambda - \beta_1 S(t)E(t) - \beta_2 S(t)I(t) - (\mu + \rho)S(t), \\ \dfrac{dE(t)}{dt} = \beta_1 S(t)E(t) + \beta_2 S(t)I(t) - (\gamma + \rho)E(t), \\ \dfrac{dI(t)}{dt} = \gamma E(t) - (\delta + \rho)I(t), \\ \dfrac{dQ(t)}{dt} = \delta I(t) - (\theta + \rho + \eta)Q(t), \\ \dfrac{dR(t)}{dt} = \theta Q(t) - \rho R(t), \\ \dfrac{dP(t)}{dt} = \mu S(t) - \rho P(t), \\ \dfrac{dD(t)}{dt} = \eta Q(t), \end{cases} \tag{4}$$

where meanings of the biological parameters are given in Table 1. All the initial conditions $S(0)$, $E(0)$, $I(0)$, $Q(0)$, $R(0)$, $P(0)$, $D(0)$ are nonnegative.

To observe influence of memory effects, by integrating both side of system (4), and then a system of integral equations is

Table 2
Four cases in model (8).

Name	Condition	Derivative or integral terms	
		Left-hand	Right-hand
Model 1	$\alpha_1 = \alpha_2 = 1$	Integer-order derivatives	No
Model 2	$0 < \alpha_1 = \alpha_2 < 1$	Fractional derivatives	No
Model 3	$0 < \alpha_1 < 1, 0 < \alpha_2 - \alpha_1 < 1$	Fractional derivatives	Fractional integrals
Model 4	$0 < \alpha_2 < \alpha_1 < 1$	Fractional derivatives	Fractional derivatives

obtained. After that, we fractionalize the integrals with time-dependent functions

$$\begin{cases} S(t) - S(0) = \int_0^t \kappa_1(t-\tau)\left[\Lambda - \beta_1 S(\tau)E(\tau) \right. \\ \quad \left. - \beta_2 S(\tau)I(\tau) - (\mu+\rho)S(\tau)\right]\mathrm{d}\tau, \\ E(t) - E(0) = \int_0^t \kappa_1(t-\tau)\left[\beta_1 S(\tau)E(\tau) + \beta_2 S(\tau)I(\tau) \right. \\ \quad \left. - (\gamma+\rho)E(\tau)\right]\mathrm{d}\tau, \\ I(t) - I(0) = \int_0^t \kappa_1(t-\tau)\left[\gamma E(\tau) - (\delta+\rho)I(\tau)\right]\mathrm{d}\tau, \\ Q(t) - Q(0) = \int_0^t \kappa_1(t-\tau)\left[\delta I(\tau) - (\rho+\eta)Q(\tau)\right]\mathrm{d}\tau \\ \quad - \theta\int_0^t \kappa_2(t-\tau)Q(\tau)\mathrm{d}\tau, \\ R(t) - R(0) = \theta\int_0^t \kappa_2(t-\tau)Q(\tau)\mathrm{d}\tau - \rho\int_0^t \kappa_1(t-\tau)R(\tau)\mathrm{d}\tau, \\ P(t) - P(0) = \mu\int_0^t \kappa_1(t-\tau)S(\tau)\mathrm{d}\tau - \rho\int_0^t \kappa_1(t-\tau)P(\tau)\mathrm{d}\tau, \\ D(t) - D(0) = \eta\int_0^t \kappa_1(t-\tau)Q(\tau)\mathrm{d}\tau, \end{cases} \tag{5}$$

where time-dependent kernels $\kappa_i(t-\tau), i = 1, 2$ have an important role in describing long memory effects. When $\kappa_i(t-\tau) = 1$, the model is classical Markov processes and memoryless. In fact, kernel functions can be replaced by any arbitrary function. A proper choice is power-law function which exhibits a slow decay such that early states also contribute to evolution of the model. It is obvious that the living quarantined cases $Q(t)$ have different memory effects. Thus, time-dependent kernels can naturally choose as the following power law functions:

$$\kappa_i(t-\tau) = \frac{1}{\Gamma(\alpha_i)}(t-\tau)^{\alpha_i - 1}, i = 1, 2, \tag{6}$$

where $\alpha_i > 0$. Substituting (6) into (5) and using Definition 1, we obtain

$$\begin{cases} S(t) - S(0) = \mathcal{I}_{0,t}^{\alpha_1}\left[\Lambda - \beta_1 S(t)E(t) - \beta_2 S(t)I(t) - (\mu+\rho)S(t)\right], \\ E(t) - E(0) = \mathcal{I}_{0,t}^{\alpha_1}\left[\beta_1 S(t)E(t) + \beta_2 S(t)I(t) - (\gamma+\rho)E(t)\right], \\ I(t) - I(0) = \mathcal{I}_{0,t}^{\alpha_1}\left[\gamma E(t) - (\delta+\rho)I(t)\right], \\ Q(t) - Q(0) = \mathcal{I}_{0,t}^{\alpha_1}\left[\delta I(t) - (\rho+\eta)Q(t)\right] - \theta\mathcal{I}_{0,t}^{\alpha_2}Q(t), \\ R(t) - R(0) = \theta\mathcal{I}_{0,t}^{\alpha_2}Q(t) - \rho\mathcal{I}_{0,t}^{\alpha_1}R(t), \\ P(t) - P(0) = \mathcal{I}_{0,t}^{\alpha_1}\left(\mu S(t) - \rho P(t)\right), \\ D(t) - D(0) = \eta\mathcal{I}_{0,t}^{\alpha_1}Q(t). \end{cases} \tag{7}$$

The decaying rate of the memory kernel depends on order α_i. A smaller value of α_i corresponds to a slower decay rate. Taking the Caputo fractional derivative of order α_1 on both sides of system (7), we derive a two-side fractional generalized SEIR model as follows,

$$\begin{cases} {}_C\mathcal{D}_{0,t}^{\alpha_1}S(t) = \Lambda - \beta_1 S(t)E(t) - \beta_2 S(t)I(t) - (\mu+\rho)S(t), \\ {}_C\mathcal{D}_{0,t}^{\alpha_1}E(t) = \beta_1 S(t)E(t) + \beta_2 S(t)I(t) - (\gamma+\rho)E(t), \\ {}_C\mathcal{D}_{0,t}^{\alpha_1}I(t) = \gamma E(t) - (\delta+\rho)I(t), \\ {}_C\mathcal{D}_{0,t}^{\alpha_1}Q(t) = \delta I(t) - \theta\mathscr{D}_{0,t}^{\alpha_1-\alpha_2}Q(t) - (\rho+\eta)Q(t), \\ {}_C\mathcal{D}_{0,t}^{\alpha_1}R(t) = \theta\mathscr{D}_{0,t}^{\alpha_1-\alpha_2}Q(t) - \rho R(t), \\ {}_C\mathcal{D}_{0,t}^{\alpha_1}P(t) = \mu S(t) - \rho P(t), \\ {}_C\mathcal{D}_{0,t}^{\alpha_1}D(t) = \eta Q(t), \end{cases} \tag{8}$$

where $\mathscr{D}_{0,t}^{\alpha_1-\alpha_2} = {}_C\mathcal{D}_{0,t}^{\alpha_1}\mathcal{I}_{0,t}^{\alpha_2}$ and $0 < \alpha_i < 1, i = 1, 2$. When $\alpha_1 < \alpha_2$, equation $\mathscr{D}_{0,t}^{\alpha_1-\alpha_2}Q(t) = {}_C\mathcal{D}_{0,t}^{\alpha_1}\mathcal{I}_{0,t}^{\alpha_2}Q(t) = {}_C\mathcal{D}_{0,t}^{\alpha_1}\mathcal{I}_{0,t}^{\alpha_1}\mathcal{I}_{0,t}^{\alpha_2-\alpha_1}Q(t) = \mathcal{I}_{0,t}^{\alpha_2-\alpha_1}Q(t)$ is a fractional integral term, then system (8) includes fractional derivative terms on left and fractional integral terms on right. When $\alpha_2 = \alpha_1$, that is $\mathscr{D}_{0,t}^{\alpha_1-\alpha_2}Q(t) = Q(t)$, system (8) is a fractional generalized SEIR model with the same memory. When $\alpha_1 > \alpha_2$, equation $\mathscr{D}_{0,t}^{\alpha_1-\alpha_2}Q(t) = {}_C\mathcal{D}_{0,t}^{\alpha_1-\alpha_2}\left({}_C\mathcal{D}_{0,t}^{\alpha_2}\mathcal{I}_{0,t}^{\alpha_2}Q(t)\right) = {}_C\mathcal{D}_{0,t}^{\alpha_1-\alpha_2}Q(t)$ is a Caputo fractional derivative term, then system (8) includes fractional derivative terms. Thus, the model (8) includes four cases, which are listed in Table 2.

4. Dynamical analysis

To qualitatively analyze characteristics of the infectious diseases, we examine dynamic behaviors of the model (8). Because right-hand side of the model (8) also contains fractional derivatives or integrals, it is not easy to analyze its dynamical behavior. We convert the system to a class of equivalent systems that only includes fractional derivatives on left-hand side. Dynamical analysis is subsequently discussed for the equivalent systems. The last equation in (8) is removed temporarily because it is only a receiver and is not involved in the remainder.

Basic reproduction number can predict whether the disease will become an epidemic or not, and is a critical value that depends on some parameters inherent in the disease. In model (8), the basic reproduction number is defined as

$$R_0 = \frac{\beta_1\Lambda(\delta+\rho) + \beta_2\Lambda\gamma}{(\gamma+\rho)(\delta+\rho)(\mu+\rho)}. \tag{9}$$

In the subsequent discussion, assume that $\alpha_1 = \frac{k_1}{m_1}$ and $\alpha_2 = \frac{k_2}{m_2}$ are rational numbers, where $(k_i, m_i) = 1, k_i, m_i \in \mathbb{Z}^+, i = 1, 2$. Let M be lowest common multiple of the denominators m_1 and m_2, and

$$L(\lambda) = \begin{vmatrix} \lambda^{M\alpha_1} + \beta_1 E^* + \beta_2 I^* + (\mu+\rho) & \beta_1 S^* & \beta_2 S^* \\ -\beta_1 E^* - \beta_2 I^* & \lambda^{M\alpha_1} - \beta_1 S^* + \gamma + \rho & -\beta_2 S^* \\ 0 & -\gamma & \lambda^{M\alpha_1} + \delta + \rho \end{vmatrix}.$$

4.1. Equivalent system and asymptotically stability analysis

Based on the discussion in Table 2, model (8) includes four submodels. Since stability analysis methods of the four models are almost the same, we only give detailed derivation process of Model 3.

4.1.1. Stability of model 3

If $\alpha_1 < \alpha_2$, we apply the following transformation:

$$\tilde{Q}(t) = \mathscr{D}_{0,t}^{\alpha_1-\alpha_2} Q(t) = \mathcal{I}_{0,t}^{\alpha_2-\alpha_1} Q(t), \tag{10}$$

then

$${}_C\mathcal{D}_{0,t}^{\alpha_2-\alpha_1} \tilde{Q}(t) = Q(t). \tag{11}$$

System (8) is equivalent to the following system:

$$\begin{cases} {}_C\mathcal{D}_{0,t}^{\alpha_2-\alpha_1} \tilde{Q}(t) = Q(t), \\ {}_C\mathcal{D}_{0,t}^{\alpha_1} S(t) = \Lambda - \beta_1 S(t)E(t) - \beta_2 S(t)I(t) - (\mu+\rho)S(t), \\ {}_C\mathcal{D}_{0,t}^{\alpha_1} E(t) = \beta_1 S(t)E(t) + \beta_2 S(t)I(t) - (\gamma+\rho)E(t), \\ {}_C\mathcal{D}_{0,t}^{\alpha_1} I(t) = \gamma E(t) - (\delta+\rho)I(t), \\ {}_C\mathcal{D}_{0,t}^{\alpha_1} Q(t) = \delta I(t) - (\rho+\eta)Q(t) - \theta\tilde{Q}(t), \\ {}_C\mathcal{D}_{0,t}^{\alpha_1} R(t) = \theta\tilde{Q}(t) - \rho R(t), \\ {}_C\mathcal{D}_{0,t}^{\alpha_1} P(t) = \mu S(t) - \rho P(t), \\ {}_C\mathcal{D}_{0,t}^{\alpha_1} D(t) = \eta Q(t). \end{cases} \tag{12}$$

Under $\alpha_1 < \alpha_2$ case, let

$$\begin{aligned} {}_C\mathcal{D}_{0,t}^{\alpha_1}\tilde{Q}(t) = {}_C\mathcal{D}_{0,t}^{\alpha_1} S(t) = {}_C\mathcal{D}_{0,t}^{\alpha_1} E(t) = {}_C\mathcal{D}_{0,t}^{\alpha_1} I(t) = {}_C\mathcal{D}_{0,t}^{\alpha_1} Q(t) \\ = {}_C\mathcal{D}_{0,t}^{\alpha_1} R(t) = {}_C\mathcal{D}_{0,t}^{\alpha_1} P(t) = 0, \end{aligned}$$

we can obtain equilibrium points. Fractional GSEIR model (12) has at most two equilibrium points:

1. Disease free equilibrium $P_F = (\tilde{Q}^*, S^*, E^*, I^*, Q^*, R^*, P^*) = (0, \frac{\Lambda}{\mu+\rho}, 0, 0, 0, 0, \frac{\mu\Lambda}{\rho(\mu+\rho)})$.

2. Endemic equilibrium point $P_E = (\tilde{Q}^*, S^*, E^*, I^*, Q^*, R^*, P^*)$, where

$$\tilde{Q}^* = \frac{\delta\gamma}{\theta(\delta+\rho)}E^*, \quad S^* = \frac{\Lambda - (\gamma+\rho)E^*}{\mu+\rho}, \quad I^* = \frac{\gamma}{\delta+\rho}E^*,$$
$$Q^* = 0, \quad R^* = \frac{\delta\gamma}{\rho(\delta+\rho)}E^*, \quad P^* = \frac{\mu[\Lambda - (\gamma+\rho)E^*]}{\rho(\mu+\rho)}.$$

and from the third equation of (12),

$$E^* = \frac{(\mu+\rho)(\delta+\rho)}{\beta_1(\delta+\rho)+\beta_2\gamma}(R_0 - 1).$$

From (9), the endemic equilibrium point $P_E = (\tilde{Q}^*, S^*, E^*, I^*, Q^*, R^*, P^*)$ exists if and only if $R_0 > 1$.

Theorem 1. *If $R_0 < 1$, all eigenvalues obtained from equations*

$$\lambda^{M\alpha_2} + (\rho+\eta)\lambda^{M(\alpha_2-\alpha_1)} + \theta = 0 \tag{13}$$

and

$$\lambda^{2M\alpha_1} + \left(-\beta_1 S^* + \gamma + 2\rho + \delta\right)\lambda^{M\alpha_1} + (-\beta_1 S^* + \gamma + \rho)(\delta+\rho) - \beta_2\gamma S^* = 0 \tag{14}$$

satisfy conditions $|arg(\lambda)| > \frac{\pi}{2M}$, the disease free equilibrium point P_F of model (12) is locally asymptotically stable. If $R_0 > 1$, the disease-free equilibrium point P_E is unstable.

Proof. The Jacobian matrix of model (12) is given by

$$J = \begin{bmatrix} 0 & 0 & 0 & 0 & 1 & 0 & 0 \\ 0 & -\beta_1 E - \beta_2 I - (\mu+\rho) & -\beta_1 S & -\beta_2 S & 0 & 0 & 0 \\ 0 & \beta_1 E + \beta_2 I & \beta_1 S - (\gamma+\rho) & \beta_2 S & 0 & 0 & 0 \\ 0 & 0 & \gamma & -(\delta+\rho) & 0 & 0 & 0 \\ -\theta & 0 & 0 & \delta & -(\rho+\eta) & 0 & 0 \\ \theta & 0 & 0 & 0 & 0 & -\rho & 0 \\ 0 & \mu & 0 & 0 & 0 & 0 & -\rho \end{bmatrix}. \tag{15}$$

The Jacobian matrix is evaluated at P_F,

$$J^* = \begin{bmatrix} 0 & 0 & 0 & 0 & 1 & 0 & 0 \\ 0 & -(\mu+\rho) & -\beta_1 S^* & -\beta_2 S^* & 0 & 0 & 0 \\ 0 & 0 & \beta_1 S^* - (\gamma+\rho) & \beta_2 S^* & 0 & 0 & 0 \\ 0 & 0 & \gamma & -(\delta+\rho) & 0 & 0 & 0 \\ -\theta & 0 & 0 & \delta & -(\rho+\eta) & 0 & 0 \\ \theta & 0 & 0 & 0 & 0 & -\rho & 0 \\ 0 & \mu & 0 & 0 & 0 & 0 & -\rho \end{bmatrix}. \tag{16}$$

From Lemma 1, the characteristic equation is obtained from

$$\begin{aligned} &\det\left(\mathrm{diag}\left(\lambda^{M(\alpha_2-\alpha_1)}, \lambda^{M\alpha_1}, \lambda^{M\alpha_1}, \lambda^{M\alpha_1}, \lambda^{M\alpha_1}, \lambda^{M\alpha_1}, \lambda^{M\alpha_1}\right) - J^*\right) \\ =&(\lambda^{M\alpha_1} + \rho)^2(\lambda^{M\alpha_1} + \mu + \rho)[\lambda^{M\alpha_2} + (\rho+\eta)\lambda^{M(\alpha_2-\alpha_1)} + \theta] \\ &\cdot [(\lambda^{M\alpha_1} - \beta_1 S^* + \gamma + \rho)(\lambda^{M\alpha_1} + \delta + \rho) - \beta_2\gamma S^*] \\ =&0. \end{aligned} \tag{17}$$

Eigenvalues are obtained from the following equations:

$$\lambda^{M\alpha_1} = -\rho, \tag{18}$$
$$\lambda^{M\alpha_1} = -\mu - \rho, \tag{19}$$
$$\lambda^{M\alpha_2} + (\rho+\eta)\lambda^{M(\alpha_2-\alpha_1)} + \theta = 0, \tag{20}$$

and

$$\begin{aligned} &(\lambda^{M\alpha_1} - \beta_1 S^* + \gamma + \rho)(\lambda^{M\alpha_1} + \delta + \rho) - \beta_2\gamma S^* \\ =&\lambda^{2M\alpha_1} + \left(-\beta_1 S^* + \gamma + 2\rho + \delta\right)\lambda^{M\alpha_1} \\ &+ (-\beta_{S^*} + \gamma + \rho)(\delta+\rho) - \beta_2\gamma S^* \\ =&\lambda^{2M\alpha_1} + \left(-\beta_1 S^* + \gamma + 2\rho + \delta\right)\lambda^{M\alpha_1} \\ &+ (\gamma+\rho)(\delta+\rho)(1 - R_0) \\ =&0. \end{aligned} \tag{21}$$

By De-Moivre formulas, arguments of roots of (18) and (19) have the form

$$\arg(\lambda_n) = \frac{\pi}{M\alpha_1} + \frac{2n\pi}{M\alpha_1}, \quad n = 0, 1, 2, \ldots, M\alpha_1 - 1.$$

Hence, $\arg(\lambda_n) > \frac{\pi}{2M}$. If $R_0 < 1$, according to Descartes' rule of sign [21], all coefficients of (20) and (21) are positive real numbers. Eqs. (20) and (21) do not have positive real roots, and roots are composed of negative real numbers and/or complex conjugate numbers. Furthermore, from (13) and (14), by Lemma 1, the disease-free equilibrium P_F of system (12) is locally asymptotically stable. □

Theorem 2. *With regard to model (12), assume that $R_0 > 1$, and all roots of equations*

$$\lambda^{M\alpha_2} + (\delta+\rho)\lambda^{M(\alpha_2-\alpha_1)} + \theta = 0 \text{ and } L(\lambda) = 0$$

satisfy conditions $|arg(\lambda)| > \frac{\pi}{2M}$, the endemic equilibrium point P_F of system (12) is locally asymptotically stable.

Proof. When (15) is evaluated at P_F, eigenvalues are derived from the following equation:

$$(\lambda^{M\alpha_1} + \rho)^2[\lambda^{M\alpha_2} + (\delta+\rho)\lambda^{M(\alpha_2-\alpha_1)} + \theta] \cdot L(\lambda) = 0. \tag{22}$$

Therefore, eigenvalues are obtained from $\lambda^{M\alpha_1} = -\rho$. By De-Moivre formulas, eigenvalues $\lambda^{M\alpha_1}$ do not influence the stability conditions of P_F. Consequently, the endemic equilibrium point P_F is asymptotically stable in terms of Lemma 1. □

4.1.2. Stability of models 1 and 2

If $\alpha_1 = \alpha_2 \leq 1$, system (8) is equivalent to the following system:

$$\begin{cases} {}_C\mathcal{D}_{0,t}^{\alpha_1} S(t) = \Lambda - \beta_1 S(t)E(t) - \beta_2 S(t)I(t) - (\mu+\rho)S(t), \\ {}_C\mathcal{D}_{0,t}^{\alpha_1} E(t) = \beta_1 S(t)E(t) + \beta_2 S(t)I(t) - (\gamma+\rho)E(t), \\ {}_C\mathcal{D}_{0,t}^{\alpha_1} I(t) = \gamma E(t) - (\delta+\rho)I(t), \\ {}_C\mathcal{D}_{0,t}^{\alpha_1} Q(t) = \delta I(t) - (\rho+\eta)Q(t) - \theta Q(t), \\ {}_C\mathcal{D}_{0,t}^{\alpha_1} R(t) = \theta Q(t) - \rho R(t), \\ {}_C\mathcal{D}_{0,t}^{\alpha_1} P(t) = \mu S(t) - \rho P(t), \\ {}_C\mathcal{D}_{0,t}^{\alpha_1} D(t) = \eta Q(t). \end{cases} \tag{23}$$

Let

$$\begin{aligned} {}_C\mathcal{D}_{0,t}^{\alpha_1} S(t) = {}_C\mathcal{D}_{0,t}^{\alpha_1} E(t) = {}_C\mathcal{D}_{0,t}^{\alpha_1} I(t) = {}_C\mathcal{D}_{0,t}^{\alpha_1} Q(t) \\ = {}_C\mathcal{D}_{0,t}^{\alpha_1} R(t) = {}_C\mathcal{D}_{0,t}^{\alpha_1} P(t) = 0, \end{aligned}$$

we can get that the fractional GSEIR model (23) has at most two equilibrium points:

1. Disease free equilibrium point $P_F = (S^*, E^*, I^*, Q^*, R^*, P^*) = (\frac{\Lambda}{\mu+\rho}, 0, 0, 0, 0, \frac{\mu\Lambda}{\rho(\mu+\rho)})$.
2. Endemic equilibrium point $P_E = (S^*, E^*, I^*, Q^*, R^*, P^*)$, where

$$\begin{aligned} &S^* = \frac{\Lambda - (\gamma+\rho)E^*}{\mu+\rho}, \quad E^* = \frac{(\mu+\rho)(\delta+\rho)}{\beta_1(\delta+\rho)+\beta_2\gamma}(R_0 - 1), \\ &I^* = \frac{\gamma}{\delta+\rho}E^*, \\ &Q^* = \frac{\gamma\delta}{(\eta+\theta+\rho)(\delta+\rho)}E^*, \quad R^* = \frac{\gamma\delta\theta}{\rho(\eta+\theta+\rho)(\delta+\rho)}E^*, \\ &P^* = \frac{\mu[\Lambda - (\gamma+\rho)E^*]}{\rho(\mu+\rho)}. \end{aligned}$$

The endemic equilibrium point exists when $R_0 > 1$.

Similar to $\alpha_1 < \alpha_2$ case, using Lemma 2, we could get the following two theorems.

Theorem 3. *If $R_0 < 1$, the disease-free equilibrium point P_F of system (23) is locally asymptotic stability. If $R_0 > 1$, the disease-free equilibrium point P_F of system (23) is unstable.*

Theorem 4. *With regard to model (23), assume that $R_0 > 1$, and eigenvalues λ from equation*

$$\begin{vmatrix} \lambda + \beta_1 E^* + \beta_2 I^* + (\mu+\rho) & \beta_1 S^* & \beta_2 S^* \\ -\beta_1 E^* - \beta_2 I^* & \lambda - \beta_1 S^* + \gamma + \rho & -\beta_2 S^* \\ 0 & -\gamma & \lambda + \delta + \rho \end{vmatrix} = 0$$

satisfy conditions $|arg(\lambda)| > \frac{\pi}{2M}$, the endemic equilibrium point P_F of model (23) is locally asymptotically stable.

4.1.3. Stability of model 4

Similar to $\alpha_1 < \alpha_2$ case, we could obtain the following results. If $\alpha_1 > \alpha_2$, we apply the following transformations:

$$\begin{aligned} \tilde{Q}(t) &= {}_C\mathcal{D}_{0,t}^{\alpha_2} Q(t) + \theta Q(t), \\ \tilde{R}(t) &= {}_C\mathcal{D}_{0,t}^{\alpha_2} R(t) - \theta Q(t), \end{aligned} \tag{24}$$

then

$$\begin{aligned} {}_C\mathcal{D}_{0,t}^{\alpha_1-\alpha_2}\tilde{Q}(t) &= {}_C\mathcal{D}_{0,t}^{\alpha_1} Q(t) + \theta\, {}_C\mathcal{D}_{0,t}^{\alpha_1-\alpha_2} Q(t) = \delta I(t) - (\rho+\eta)Q(t), \\ {}_C\mathcal{D}_{0,t}^{\alpha_1-\alpha_2}\tilde{R}(t) &= {}_C\mathcal{D}_{0,t}^{\alpha_1} R(t) - \theta\, {}_C\mathcal{D}_{0,t}^{\alpha_1-\alpha_2} Q(t) = -\rho R(t). \end{aligned} \tag{25}$$

From (24) and (25), (8) is equivalent to the following system:

$$\begin{cases} {}_C\mathcal{D}_{0,t}^{\alpha_1-\alpha_2}\tilde{Q}(t) = \delta I(t) - (\eta+\rho)Q(t), \\ {}_C\mathcal{D}_{0,t}^{\alpha_1-\alpha_2}\tilde{R}(t) = -\rho R(t), \\ {}_C\mathcal{D}_{0,t}^{\alpha_1} S(t) = \Lambda - \beta_1 S(t)E(t) - \beta_2 S(t)I(t) - (\mu+\rho)S(t), \\ {}_C\mathcal{D}_{0,t}^{\alpha_1} E(t) = \beta_1 S(t)E(t) + \beta_2 S(t)I(t) - (\gamma+\rho)E(t), \\ {}_C\mathcal{D}_{0,t}^{\alpha_1} I(t) = \gamma E(t) - (\delta+\rho)I(t), \\ {}_C\mathcal{D}_{0,t}^{\alpha_2} Q(t) = \tilde{Q}(t) - \theta Q(t), \\ {}_C\mathcal{D}_{0,t}^{\alpha_2} R(t) = \tilde{R}(t) + \theta Q(t), \\ {}_C\mathcal{D}_{0,t}^{\alpha_1} P(t) = \mu S(t) - \rho P(t), \\ {}_C\mathcal{D}_{0,t}^{\alpha_1} D(t) = \eta Q(t). \end{cases} \tag{26}$$

Let

$$\begin{aligned} {}_C\mathcal{D}_{0,t}^{\alpha_1-\alpha_2}\tilde{Q}(t) = {}_C\mathcal{D}_{0,t}^{\alpha_1-\alpha_2}\tilde{R}(t) = {}_C\mathcal{D}_{0,t}^{\alpha_1} S(t) = {}_C\mathcal{D}_{0,t}^{\alpha_1} E(t) \\ = {}_C\mathcal{D}_{0,t}^{\alpha_1} I(t) = {}_C\mathcal{D}_{0,t}^{\alpha_2} Q(t) = {}_C\mathcal{D}_{0,t}^{\alpha_2} R(t) \\ = {}_C\mathcal{D}_{0,t}^{\alpha_1} P(t) = 0, \end{aligned}$$

we can get that the fractional GSEIR model (23) has at most two equilibrium points:

1. Disease free equilibrium point $P_F = (\tilde{Q}^*, \tilde{R}^*, S^*, E^*, I^*, Q^*, R^*, P^*) = (0, 0, \frac{\Lambda}{\mu+\rho}, 0, 0, 0, 0, \frac{\mu\Lambda}{\rho(\mu+\rho)})$.
2. Endemic equilibrium point $P_E = (\tilde{Q}^*, \tilde{R}^*, S^*, E^*, I^*, Q^*, R^*, P^*)$, where

$$\begin{aligned} &\tilde{Q}^* = \frac{\theta\gamma\delta}{(\eta+\rho)(\delta+\rho)}E^*, \quad \tilde{R}^* = -\frac{\theta\gamma\delta}{(\eta+\rho)(\delta+\rho)}E^*, \\ &S^* = \frac{\Lambda - (\gamma+\rho)E^*}{\mu+\rho}, \quad I^* = \frac{\gamma}{\delta+\rho}E^*, \\ &E^* = \frac{(\mu+\rho)(\delta+\rho)}{\beta_1(\delta+\rho)+\beta_2\gamma}(R_0 - 1), Q^* = \frac{\gamma\delta}{(\eta+\rho)(\delta+\rho)}E^*, \\ &R^* = 0, \quad P^* = \frac{\mu[\Lambda - (\gamma+\rho)E^*]}{\rho(\mu+\rho)}. \end{aligned}$$

The endemic equilibrium point exists when $R_0 > 1$.

Theorem 5. *If $R_0 < 1$, all roots from equations*

$$\lambda^{M\alpha_1} + \theta\lambda^{M(\alpha_1-\alpha_2)} + \rho + \eta = 0 \tag{27}$$

and

$$\begin{aligned} &\lambda^{2M\alpha_1} + \left(-\beta_1 S^* + \gamma + \delta + 2\rho\right)\lambda^{M\alpha_1} \\ &\quad + (-\beta_1 S^* + \gamma + \rho)(\delta+\rho) - \beta_2\gamma S^* = 0 \end{aligned} \tag{28}$$

satisfy conditions $|arg(\lambda)| > \frac{\pi}{2M}$, the disease free equilibrium point P_F of system (23) is locally asymptotically stable. If $R_0 > 1$, the disease-free equilibrium point P_E is unstable.

Theorem 6. *With regard to system (26), assume that $R_0 > 1$ and all roots from equations*

$$\lambda^{M\alpha_1} + \theta\lambda^{M(\alpha_1-\alpha_2)} + \rho + \eta = 0 \text{ and } L(\lambda) = 0$$

satisfy conditions $|arg(\lambda)| > \frac{\pi}{2M}$, the endemic equilibrium point P_F of system (12) is locally asymptotically stable.

4.2. Positivity and boundedness

In what follows, positivity and boundedness of the solution are given.

Theorem 7. *The model (8) with initial condition* $(S(0), E(0), I(0), Q(0), R(0), P(0)) \in \mathbb{R}^6_+$ *has a unique nonnegative solution. Moreover, the compact set*

$$\Omega = \left\{(S, E, I, Q, R, P) \in \mathbb{R}^6_+ : 0 \le S + I + R + Q + R + P \le \frac{\Lambda}{\rho}\right\} \tag{29}$$

is a positively invariant set that attracts all solutions of system (8) in $\mathbb{R}^6_+$.

Proof. Obviously, the right hand side of equivalent systems (12), (23) and (26) satisfy the local Lipschitz condition, respectively. By Lemma 3, systems (12), (23) and (26) all have unique solutions. These results indicate that system (8) has a unique solution.

Based on the fractional comparison theorem [22], it is obvious that the solution of system (8) satisfies $S(t) \ge 0, E(t) \ge 0, I(t) \ge 0, Q(t) \ge 0, R(t) \ge 0$ and $P(t) \ge 0$. Let $N(t) = S(t) + E(t) + I(t) + Q(t) + R(t) + P(t)$. Adding the first six equations in the model (8) gives

$${}_C\mathcal{D}^{\alpha_1}_{0,t} N(t) = \Lambda - \rho N(t) - \eta Q(t) \le \Lambda - \rho N(t). \tag{30}$$

By re-applying the fractional comparison theorem, we get

$$N(t) \le \left(-\frac{\Lambda}{\rho} + N(0)\right) E_{\alpha_1}(-\rho t^{\alpha_1}) + \frac{\Lambda}{\rho}. \tag{31}$$

If $N(0) \le \frac{\Lambda}{\rho}$, and noting that $E_{\alpha_1}(-\rho t^{\alpha_1}) \ge 0$, one has

$$N(t) \le \frac{\Lambda}{\rho}$$

Thus, Ω is a positively invariant set.

By $\lim_{t\to\infty} E_{\alpha_1}(-\rho t^{\alpha}) = 0$ and (31), we determine that $\lim_{t\to\infty} N(t) = \frac{\Lambda}{\rho}$. Hence, Ω attract the solution of model (8). The proof is completed. □

4.3. Sensitivity analysis

The basic reproduction number R_0 is employed to measure transmission potential of the disease. It is obvious that relationship between R_0 and each parameter is expressed as follows,

$$\frac{\partial R_0}{\partial \Lambda} > 0, \frac{\partial R_0}{\partial \beta_1} > 0, \frac{\partial R_0}{\partial \beta_2} > 0, \frac{\partial R_0}{\partial \mu} < 0, \frac{\partial R_0}{\partial \gamma} < 0, \frac{\partial R_0}{\partial \delta} < 0, \frac{\partial R_0}{\partial \rho} < 0.$$

Therefore R_0 is increasing with $\Lambda, \beta_1, \beta_2$ and is decreasing with $\mu, \gamma, \delta, \rho$.

Partial Rank Correlation Coefficient (PRCC) [23] is employed to further study sensitivity analysis of R_0. The magnitude of the PRCC indicates significance or importance of the parameter in contribution to the spread of newly infected population. PRCC and the corresponding p-values are calculated, and a total of 20,000 simulations per the Latin Hypercube Sampling run are carried out. When performing parameter sampling, a uniform distribution is chosen as prior distribution. The parameters and R_0 in (9) are set as input variables and output variable, respectively. The larger is absolute value of the PRCC, the greater is influence of the parameter in R_0. If the p value is greater than 0.05, the parameter is not significant for R_0.

The PRCC values of the estimated parameters associated with R_0 are listed in Table 3. From Table 3 and Fig. 3, the values reflect correlation between the parameters $\Lambda, \beta_1, \beta_2, \mu, \rho, \gamma, \delta$ and R_0. It is obvious that $\Lambda, \beta_1, \beta_2$ are positively correlated, while $\mu, \rho, \gamma, \delta$ are negatively correlated. When the infection rates β_1, β_2, the average latent time γ^{-1}, and the average quarantine time δ^{-1} increase, the value of R_0 increase, and then more individuals become infected. Furthermore, we can determine that $|\text{PRCC}(\mu)| > |\text{PRCC}(\delta)| > |\text{PRCC}(\beta_2)| > |\text{PRCC}(\Lambda)| > |\text{PRCC}(\beta_1)| > |\text{PRCC}(\gamma)| > |\text{PRCC}(\rho)|$, namely, μ is the most influential parameters in reducing R_0. The protection rate μ has the greatest negative impact on R_0, which indicates that the value of R_0 decreases quickly if large number of individuals are protected from contact with infected people. That is, the most effective way to combat COVID-19 is to increase rate of the protection μ, such as isolation and staying at home.

Table 3
The PRCC values and p-values of the estimated parameters with respect to R_0.

Input parameter	Range	PRCC values	p-value
Λ	(0.001,0.02)	0.1637	3.49e−120
β_1	(0.001,1)	0.1209	4.75e−66
β_2	(1,3)	0.2171	6.56e−212
μ	(0.001,0.5)	−0.6669	0
ρ	(0.0001,0.0004)	−0.0040	0.57
γ	(0.07,0.5)	−0.0852	1.61e−33
δ	(0.001,0.5)	−0.5606	0

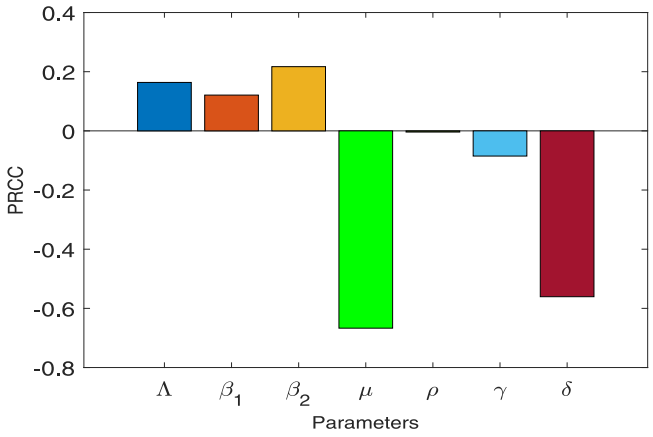

Fig. 3. The sensitivity analysis of R_0.

5. Analysis and results

5.1. Data sources

In this paper, the data of COVID-19 is from the Johns Hopkins University Center for Systems Science and Engineering (https://github.com/CSSEGISandData/COVID-19). The data include accumulated and newly confirmed cases, recovered cases and death cases worldwide since January 22, 2020. In order to further illustrate the effectiveness of the model, we add SEIR [5] and SEIR+PO [24] models to compare with our model.

The initial values of models are obtained from the data beside the total population. We calculate parameters and numerical approximate solutions of model (8) by Simulink Design Optimization of MATLAB. We can identify the parameters in the model (8) via fractional Adams–Bashforth–Moulton method and nonlinear least squares. The program is available at: https://github.com/WeiyuanMa/matlab-program.git.

5.2. Epidemic progression and analysis in the United States

Based on the reported data from February 24 to May 30, 2020 in the United States, the best-fit values of the parameters are listed in Table 4. The R_0 values of Models 1, 2, 3 and 4 are 1.0268, 1.0008, 0.8771 and 0.9199, respectively. Clearly, the disease is still in the midst of an outbreak, and the model can fit the real data well. For comparison, the newly reported data from May 31 to June 9, 2020 are marked differently in Fig. 4. As shown in Figs. 4

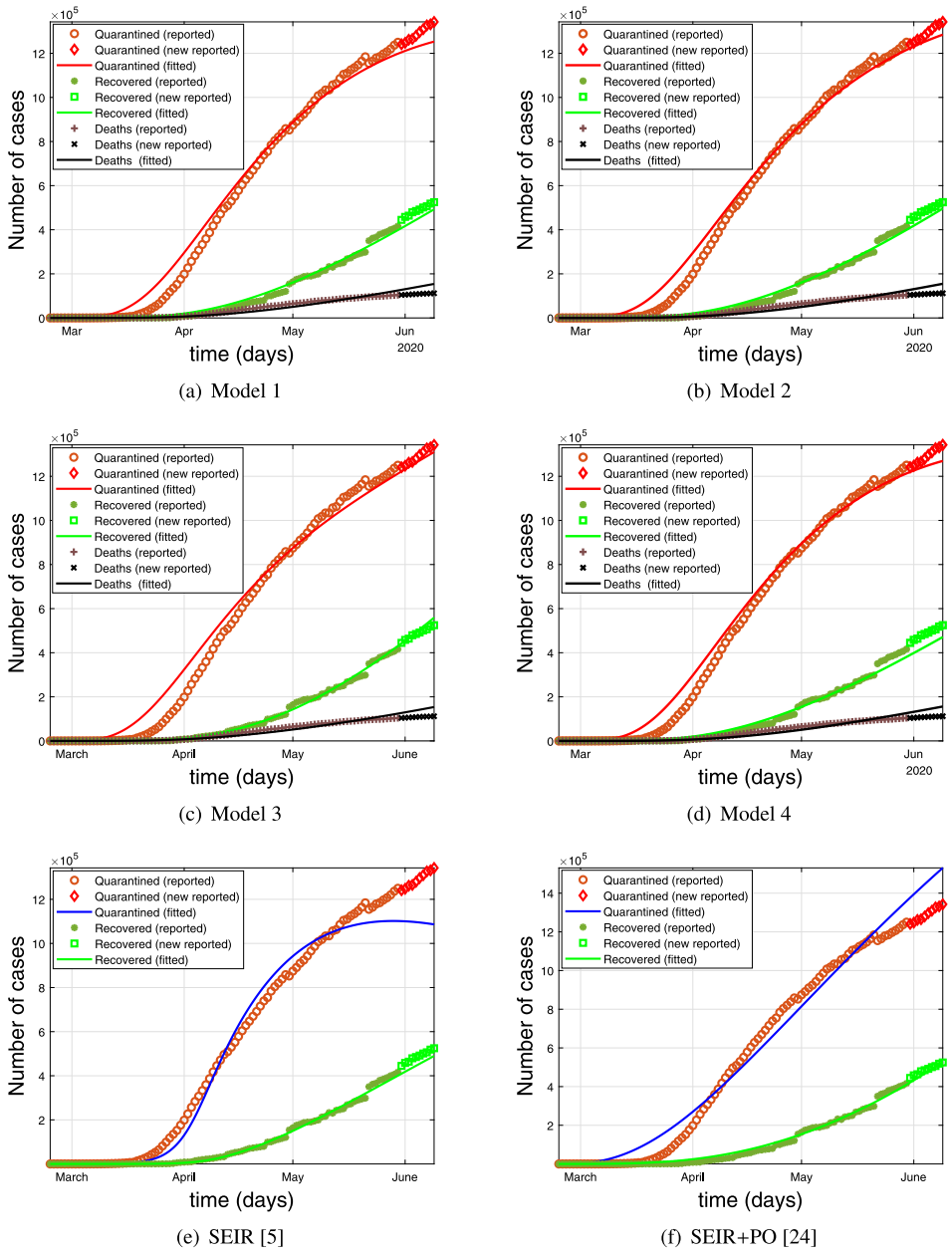

(a) Model 1 (b) Model 2

(c) Model 3 (d) Model 4

(e) SEIR [5] (f) SEIR+PO [24]

Fig. 4. Forecast of COVID-19 epidemics in the United States (data from February 24 to May 30, 2020 are used for modeling fitting, while the rest 10 data form May 31 to June 9 are used for validation).

Table 4
Identified parameters by least squares fitting in the United States.

Parameter	Model 1	Model 2	Model 3	Model 4
Λ	0.0092	0.0057	0.02347	0.0148
β_1	1.6594	2.310	0.2480	0.1473
β_2	0.6145	0.6373	1.0504	1.0411
μ	0.1048	0.1221	0.0507	0.1071
ρ	0.0001	0.0001	0.0644	1.0674e−05
γ	0.1848	0.1335	0.1632	0.1753
δ	0.2296	0.1534	0.1702	0.1800
η	0.0024	0.0024	0.0025	0.0024
θ	0.0077	0.0079	0.0008	0.0078
α_1	1.0000	0.9012	0.5832	0.9273
α_2	1.0000	0.9012	0.7495	0.8702

and 5, the predicted values of cumulative confirmed cases fall within range of 95%–105% of the real values by model (8) from May 31 to June 9. However, the prediction accuracy of models SEIR and SEIR is relatively poor. Particularly, average relative errors of Models 1, 2, 3, 4, SEIR and SEIR+PO are 4.19%, 2.16%, 1.08%, 2.96%, 15.19% and 13.94%, respectively. It should be note that the number of quarantined cases (Q) is equal to the number of cumulative confirmed cases minus the cumulative cases of recovered (R) and deaths (D). It can be shown that the model 3 can more accurately predict the number of infected people in the next ten days. According to a large number of numerical experiments, forecasting capability of Model 3 is the best one for both the quarantined cases and the cumulative confirmed cases. In addition, We can use model 3 and its parameters to fit and predict disease transmission trends in other countries.

In the current situation, there is a very delicate trade-off between public health and economic impact of COVID-19. We use the model 3 to discuss effectiveness of non-pharmaceutical interventions. We employ 6 levels of regulation policy [25], which increase or reduces the contact rate by 10%, 25%, 40%, as shown

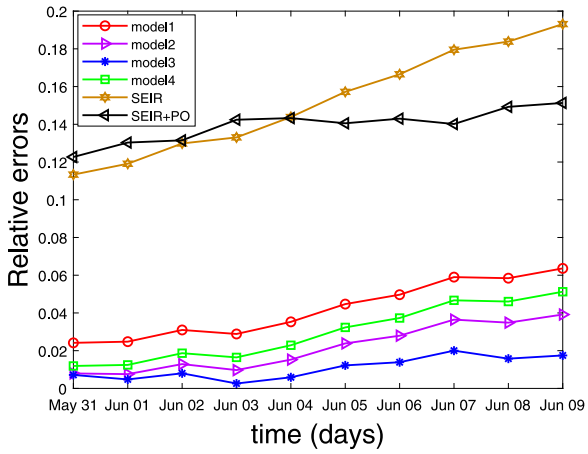

Fig. 5. Relative errors of cumulative confirmed cases from May 31 to June 9, 2020 in the United States.

Table 5
Policy regulation levels in the United States.

Regulations level	Δ from level 1	β_1	β_2	μ	δ
1	–	0.2480	1.0504	0.0507	0.1702
2	10%	0.2728	1.1554	0.0558	0.1872
3	−10%	0.2232	0.9454	0.0456	0.1532
4	25%	0.3100	1.3130	0.0634	0.2127
5	−25%	0.1860	0.7878	0.0380	0.1276
6	40%	0.3472	1.4706	0.0710	0.2383
7	−40%	0.1488	0.6302	0.0304	0.1021

in Table 5. The remaining parameters are the same as above. In Fig. 6, the predicted evolution of the quarantined cases are plotted with different infection rates β_1, β_2 levels and intervention implementation time. There is a very large difference in final number of cases predicted by the varying levels. This finding shows that relaxing current control policies can cause an alarming number of infection cases. The diffusion rate is substantially faster than deceleration rate for measures with the same magnitude. This suggests that we need to be more cautious about relaxed policy. It is visible from Fig. 7 that the quarantined cases with five protection rates μ levels and two intervention implementation times. As the rate of protection increases, the number of confirmed cases declines. When the rate of protection decreases, the number of confirmed cases increases significantly. It is also shows that increasing the rate of protection is the most effective non-pharmaceutical intervention measure. Fig. 8 shows simulation results of the different δ levels and two intervention start times. When we speed up detection, δ increases, the number of infections increase rapidly in the short term, but it speed up the end time of the disease.

5.3. Epidemic progression and analysis in Brazil

In this part, we use COVID-19 data from Brazil to further analyze validity of the model. The best-fit values of the identified parameters are listed in Table 6 by the data from February 24 to May 30, 2020. The R_0 values of the Models 1, 2, 3 and 4 are 1.3571, 1.3267, 1.7414 and 1.3704, respectively. The R_0 values greater than 1 indicates that COVID-19 is in a period of rapid spread in Brazil. As shown in Figs. 9 and 10, the models 1, 2, 3 and 4 fit really well with the real-time data. Average relative errors of Models 1, 2, 3, 4, SEIR and SEIR+PO are 4.19%, 2.16%, 1.08%, 2.96%, 15.19% and 13.94%, respectively. Obviously, model 3 has better short-term forecasting ability. Therefore, we can use Model 3 to further study the spread trends and possible policy adjustments of COVID-19.

Table 6
Identified parameters by least squares fitting in Brazil.

Parameter	Model 1	Model 2	Model 3	Model 4
Λ	0.0200	0.0280	0.0271	0.0307
β_1	1.3909	0.0705	0.2389	0.2871
β_2	0.9789	0.9691	1.0011	1.1489
μ	0.2000	0.1361	0.0782	0.1795
ρ	2.3437e−06	0.0001	0.0537	0.0001
γ	0.1892	0.1756	0.1528	0.2034
δ	0.1575	0.1602	0.0474	0.1736
η	0.0026	0.0025	0.0026	0.0026
θ	0.0224	0.0222	0.0024	0.3863
α_1	1.0000	0.9676	0.5948	0.9954
α_2	1.0000	0.9676	0.8998	0.5795

Table 7
Policy regulation levels in Brazil.

Regulations level	Δ from level 1	β_1	β_2	μ	δ
1	–	0.2389	1.0011	0.0782	0.0474
2	10%	0.2628	1.1012	0.0860	0.0521
3	−10%	0.2150	0.9010	0.0704	0.0427
4	25%	0.2986	1.2514	0.0978	0.0592
5	−25%	0.1792	0.7508	0.0587	0.0355
6	40%	0.3345	1.4015	0.1095	0.0664
7	−40%	0.1433	0.6007	0.0469	0.0284

The COVID-19 outbreak put forward a new challenge: how and when to implement control strategies. Based on the model 3, we give some further discussion. As shown in Table 7, we give 6 levels of regulation policy. The remaining parameters are the same as Table 6 in Model 3. In Fig. 11, the predicted number of infections are plotted with different infection rates β_1, β_2 levels and intervention implementation time. It is obvious that relaxing policies can lead to a sharp increase in the number of infections. The sooner strict control policies are implemented, the sooner the disease is controlled. In Fig. 12, quarantined cases are given with five protection rates μ levels and two intervention implementation times. When the protection rate increases, the number of infections goes down. In Fig. 13, simulation results are given with the different δ levels and two intervention start times. One of the things that we can conclude is that speeding up the test helps bring the end of the disease earlier.

The numerical results reveal that isolation, stay at home, strict control of social distancing, and rapid testing play a very important role in preventing the pandemic of the disease. It also turns out that when we use relaxation, the disease spreads faster. Moreover, the earlier restriction measures are used, the peak number of infections can be reduced and the disease can be controlled earlier.

6. Conclusion and discussion

In this paper, a two-side fractional generalized SEIR model (8) is proposed to investigate spread and dynamics of COVID-19. The local stability of disease-free equilibrium and endemic equilibrium are explored by the basic reproduction number R_0. Moreover, existence, uniqueness, and positivity solution of the model with initial values are established. The sensitivity analysis of R_0 to the other parameters is studied, which provides a theoretical basis for the disease control. And it also reveals that the most effective way to combat COVID-19 is to increase protection rate. Based on the least squares method and the fractional predictor–correctors algorithm, we solve inverse problem to get the best fit parameters of the model by the real data. The model suggests that we need more cautious when we take the relax measures.

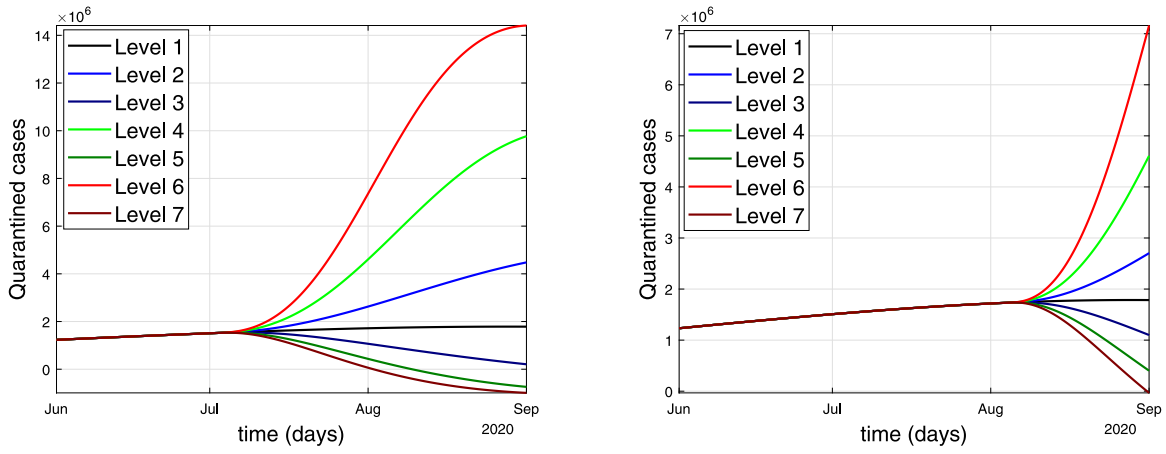

(a) Start on July 1. (b) Start on August 1.

Fig. 6. Quarantined cases with different infection rates β_1, β_2 levels and intervention implementation times in the United States.

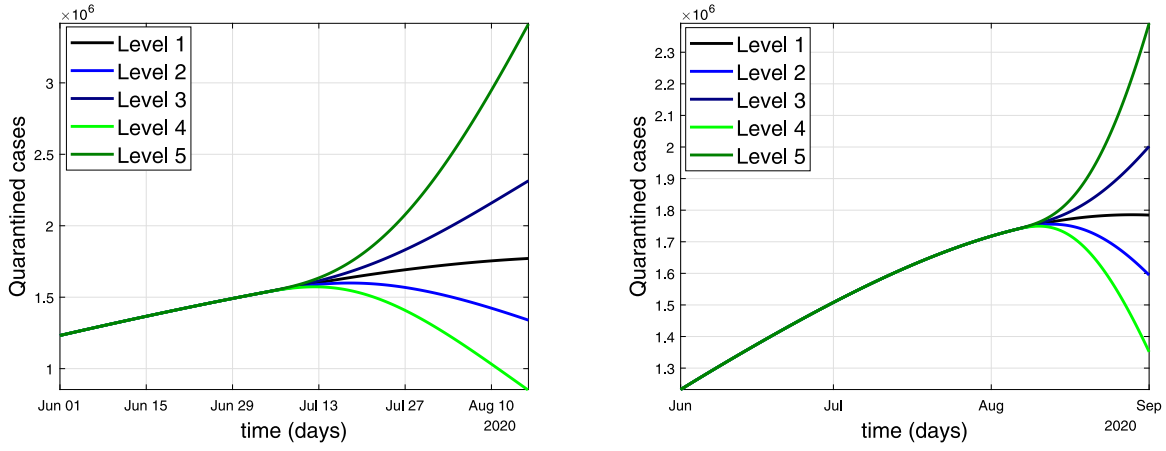

(a) Start on July 1. (b) Start on August 1.

Fig. 7. Quarantined cases with different protection rates μ levels and intervention implementation times in the United States.

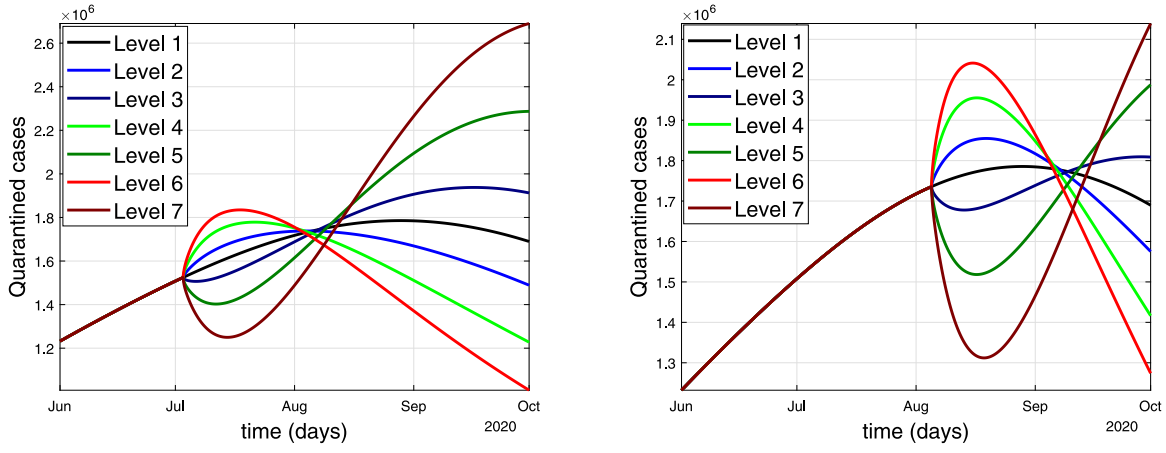

(a) Start on July 1. (b) Start on August 1.

Fig. 8. Quarantined cases with different δ levels and two intervention start times in the United States.

Finally, the advantages and disadvantages of the model are given as follows:

(a). The application of fractional calculus to infectious disease models stems from the fact that the spread of disease depends not only on the current state but also on the past state. Furthermore, the model with two-side fractional calculus has a better forecasting capabilities than the corresponding integer-order model and left-hand fractional model. Two-side fractional model can better

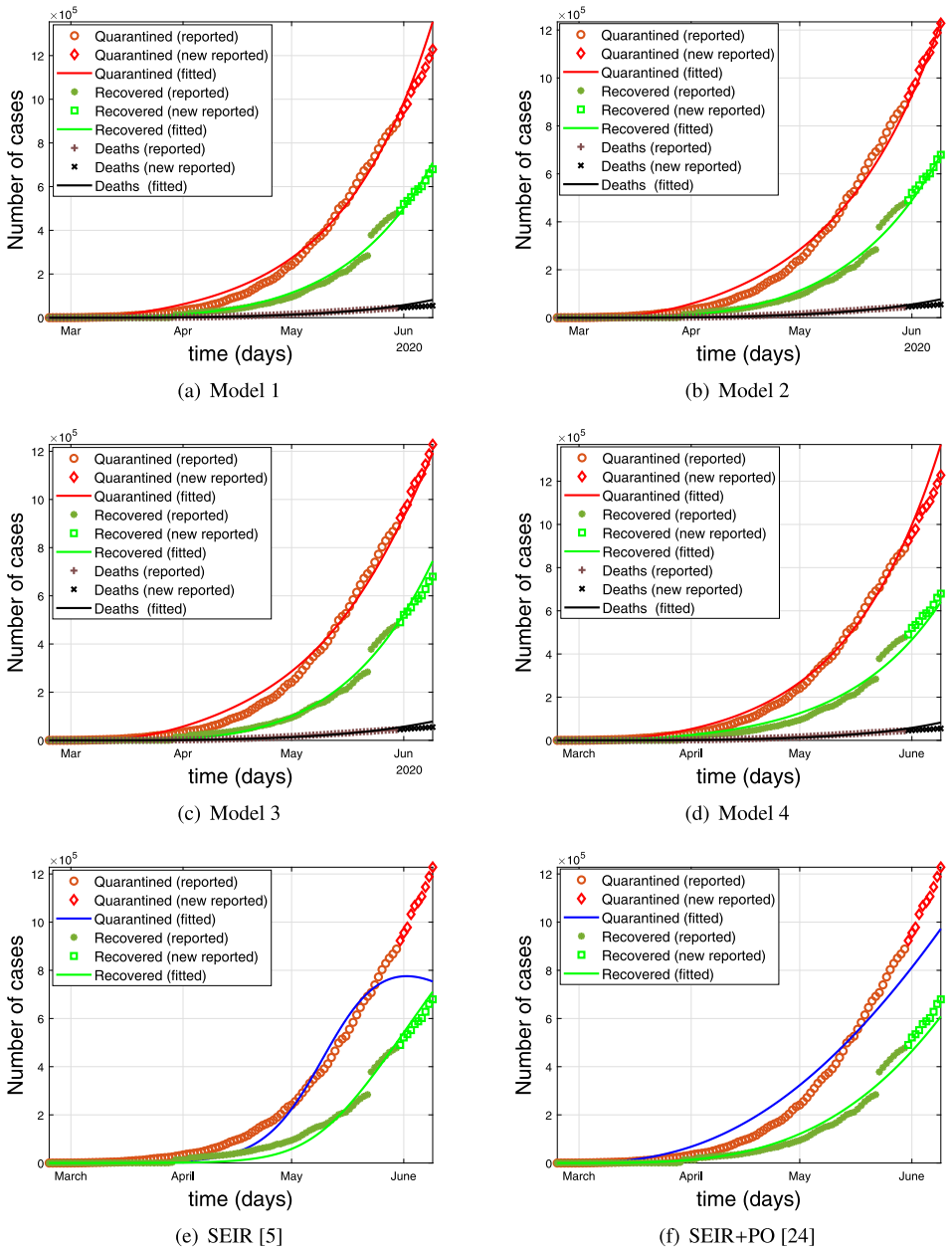

(a) Model 1 (b) Model 2

(c) Model 3 (d) Model 4

(e) SEIR [5] (f) SEIR+PO [24]

Fig. 9. Forecast of COVID-19 epidemics in Brazil (data from February 24 to May 30, 2020 are used for modeling fitting, while the rest 10 data form May 31 to June 9 are used for validation).

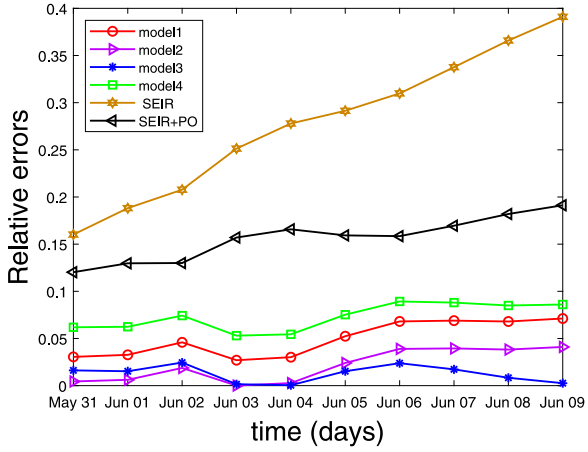

Fig. 10. Relative errors of cumulative confirmed cases from May 31 to June 9, 2020 in Brazil.

describe the heterogeneity of power-law distribution of different state variables in the model. That is the model reduces errors resulting from neglect of parameters.

(b). Due to the global dependence of fractional calculus, the computational cost of our model is higher than the corresponding integer-order model and left-hand fractional model. Besides, to get better estimation results, we build a two-side fractional model and also need to obtain the optimal parameters for the model. The parameter values and R_0 value of the model change over time due to the constant adjustment of control strategy.

(c). Due to constant adjustment of national policies, the proposed model is only suitable for short-term prediction of COVID-19 and cannot be used for long-term prediction.

With adjustment of policy and development of medical level, prediction and analysis need more elaborate models, such as, fractional age structure models, fractional models with vaccine. We will discuss it in the future work.

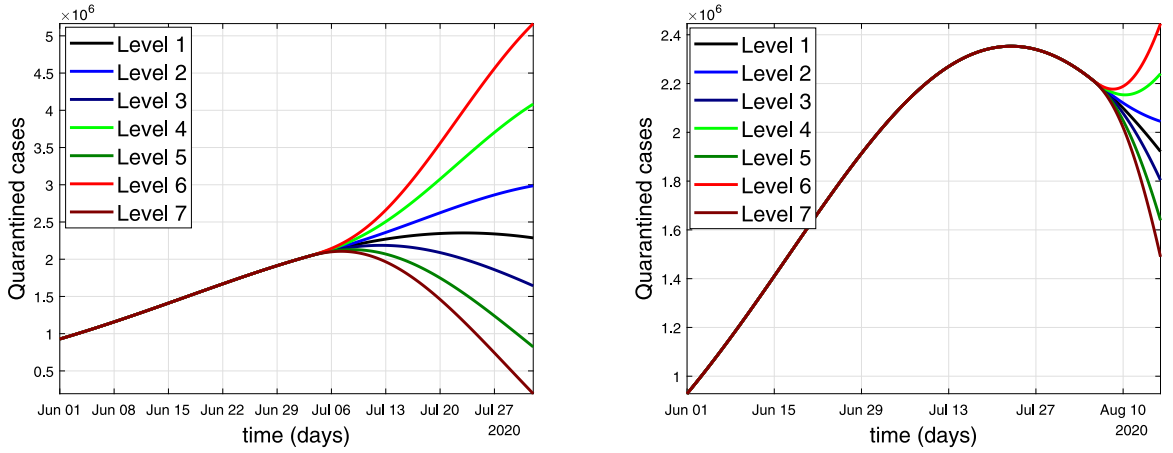

(a) Start on July 1. (b) Start on August 1.

Fig. 11. Quarantined cases with different infection rates β_1, β_2 levels and intervention implementation times in Brazil.

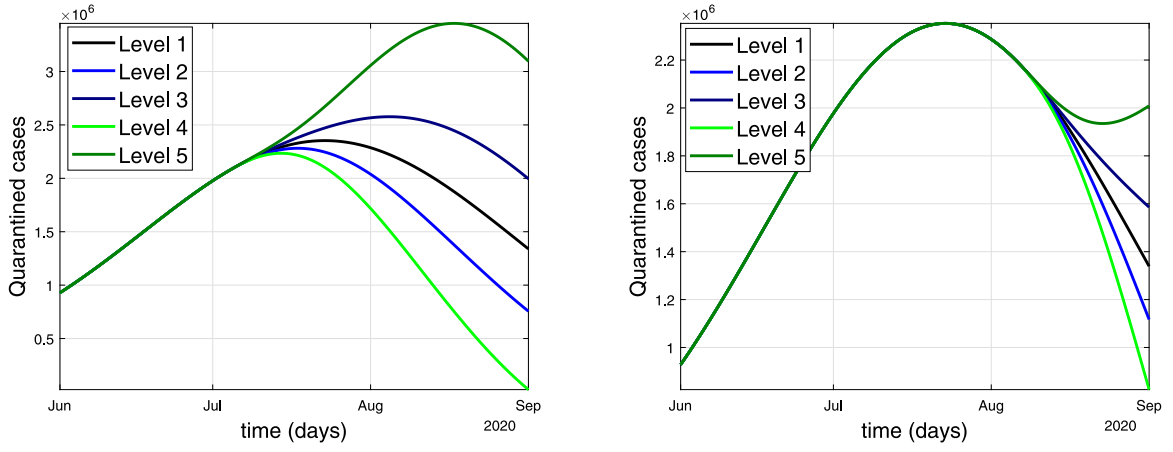

(a) Start on July 1. (b) Start on August 1.

Fig. 12. Quarantined cases with different protection rates μ levels and intervention implementation times in Brazil.

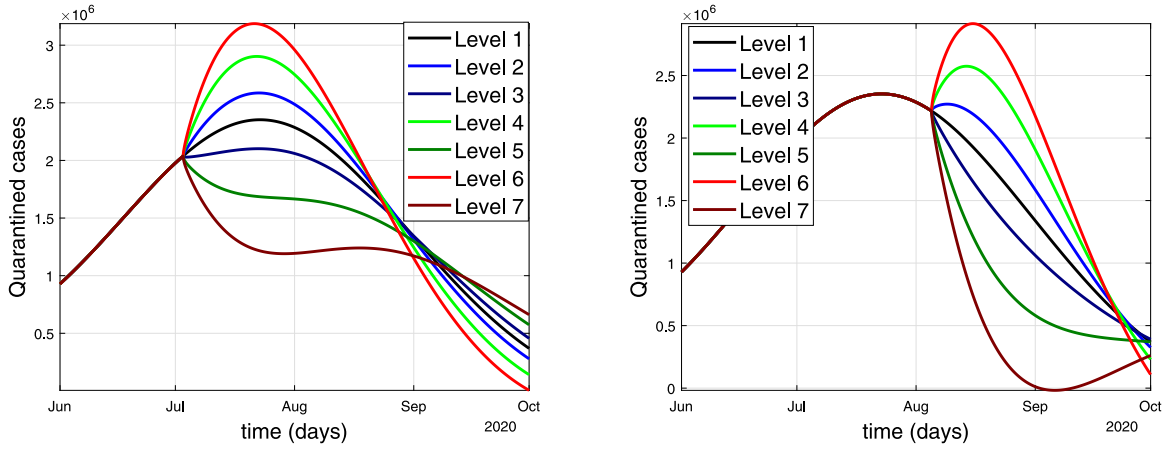

(a) Start on July 1. (b) Start on August 1.

Fig. 13. Quarantined cases with different δ levels and two intervention start times in Brazil.

Declaration of competing interest

The authors declare that they have no known competing financial interests or personal relationships that could have appeared to influence the work reported in this paper.

References

[1] World Health Organization. Coronavirus disease (COVID-2019) situation reports-153 on coronavirus disease 2019 (COVID-19) 21 2020. 2021, https://www.who.int/emergencies/diseases/novel-coronavirus-2019/situation-Reports/. [Accessed 21 June 2021].

[2] Kuniya T. Prediction of the epidemic peak of coronavirus disease in Japan, 2020. J Clin Med 2020;9(3):789.

[3] Wu JT, Leung K, Leung GM. Nowcasting and forecasting the potential domestic and international spread of the 2019-nCoV outbreak originating in Wuhan, China: a modelling study. Lancet 2020;395(10225):689.

[4] Peng L, Yang W, Zhang D, et al. Epidemic analysis of COVID-19 in China by dynamical modeling. 2020, http://dx.doi.org/10.1101/2020.02.16.20023465, medRxiv.

[5] Yang Z, Zeng Z, Wang K, et al. Modified SEIR and AI prediction of the epidemics trend of COVID-19 in China under public health interventions. J Thorac Dis 2020;12(3):165–74.

[6] Li X, Zhao X, Sun Y. The lockdown of hubei province causing different transmission dynamics of the novel coronavirus (2019-ncov) in Wuhan and Beijing. 2020, http://dx.doi.org/10.1101/2020.02.09.20021477, medRxiv.

[7] Chinazzi M, Davis JT, Ajelli M, et al. He effect of travel restrictions on the spread of the 2019 novel coronavirus (COVID-19) outbreak. Science 2020;368(6489):395–400.

[8] Boldog P, Tekeli T, Vizi Z, Dénes A, et al. Risk assessment of novel coronavirus COVID-19 outbreaks outside China. J Clin Med 2020;9(2):571.

[9] Yulmetyev RM, Emelyanova NA, Demin SA, Gafarov FM, Hänggi P, Yulmetyeva DG. Non-Markov stochastic dynamics of real epidemic process of respiratory infections. Physica A 2004;331(1–2):300–18.

[10] Agarwal P, Deniz S, Jain S, Alderremy AA, Shaban Aly. A new analysis of a partial differential equation arising in biology and population genetics via semi analytical techniques. Physica A 2020;542:122769.

[11] Podlubny I. Fractional differential equations. New York: Academic Press; 1998.

[12] Saeedian M, Khalighi M, Azimi-Tafreshi N, et al. Memory effects on epidemic evolution: The susceptible-infected-recovered epidemic model. Phys Rev E 2017;95(2):022409.

[13] Maji C, Mukherjee D, Kesh D. Study of a fractional-order model of chronic wasting disease. Math Methods Appl Sci 2020;43(7):4669–82.

[14] Rosa S, Torres DFM. Optimal control of a fractional order epidemic model with application to human respiratory syncytial virus infection. Chaos Solitons Fractals 2018;117:142–9.

[15] Xu C, Yu Y, Chen YQ, Lu ZZ. Forecast analysis of the epidemics trend of COVID-19 in the United States by a generalized fractional-order SEIR model. Nonlinear Dyn 2020;101:1621–34.

[16] Lu ZZ, Yu YG, Chen YQ, Ren GJ, et al. A fractional-order SEIHDR model for COVID-19 with inter-city networked coupling effects. Nonlinear Dyn 2020;101:1717–30.

[17] Razminia A, Majd VJ, Baleanu D. Chaotic incommensurate fractional order Rössler system: active control and synchronization. Adv Differ Equ 2011;2011(1):15.

[18] Diethelm K, Siegmund S, Tuan HT. Asymptotic behavior of solutions of linear multi-order fractional differential systems. Fract Calc Appl Anal 2017;20(5):1165–95.

[19] Li CP, Zhang FR. A survey on the stability of fractional differential equations. Eur Phys J-Spec Top 2011;193(1):27–47.

[20] Odibat ZM. Analytic study on linear systems of fractional differential equations. Comput Math Appl 2010;59(3):1171–83.

[21] Haukkanen P, Tossavainen T. A generalization of Descartes' rule of signs and fundamental theorem of algebra. Appl Math Comput 2011;218(4):1203–7.

[22] Wang Z, Yang D, Zhang H. Stability analysis on a class of nonlinear fractional-order systems. Nonlinear Dyn 2016;86(2):1023–33.

[23] Conover WJ, Conover WJ. Practical nonparametric statistics. 3rd ed.. New York: John Wiley & Sons; 1999.

[24] Yang W, Zhang D, Peng L, Zhuge C, Hong L. Rational evaluation of various epidemic models based on the COVID-19 data of China. 2020, arXiv arXiv:2003.05666.

[25] Olivier LE, Botha S, Craig IK. Optimized lockdown strategies for curbing the spread of COVID-19: A South African case study. IEEE Access 2020;8:205755-205765.